

Chiral Basis for Qubits and Spin-Helix Decay

Vladislav Popkov^{1,2}, Xin Zhang³, Frank Göhmann¹, and Andreas Klümper¹

¹*Department of Physics, University of Wuppertal, Gausstraße 20, 42119 Wuppertal, Germany*

²*Faculty of Mathematics and Physics, University of Ljubljana, Jadranska 19, SI-1000 Ljubljana, Slovenia*

³*Beijing National Laboratory for Condensed Matter Physics, Institute of Physics, Chinese Academy of Sciences, Beijing 100190, China*

 (Received 3 January 2024; revised 19 March 2024; accepted 23 April 2024; published 31 May 2024)

We propose a qubit basis composed of transverse spin helices with kinks. Unlike the usual computational basis, this chiral basis is well-suited for describing quantum states with nontrivial topology. Choosing appropriate parameters the operators of the transverse spin components, σ_n^x and σ_n^y , become diagonal in the chiral basis, which facilitates the study of problems focused on transverse spin components. As an application, we study the temporal decay of the transverse polarization of a spin helix in the XX model that has been measured in recent cold atom experiments. We obtain an explicit universal function describing the relaxation of helices of arbitrary wavelength.

DOI: [10.1103/PhysRevLett.132.220404](https://doi.org/10.1103/PhysRevLett.132.220404)

Introduction.—A proper choice of basis often is the crucial first step toward success. For example, the modes of the harmonic oscillator are best described by the coherent state basis. The use of wavelets is well-suited for describing signals confined in space or time [1], while the Fourier basis is natural for solving linear differential equations with translational invariance.

For qubits, i.e., quantum systems with spin-1/2 local degrees of freedom, the most widely used basis is the computational basis, which is composed of tensor products of the eigenstates $|0\rangle, |1\rangle$ of the σ^z operator. The advantages of the computational basis are its factorized structure, orthonormality, and $U(1)$ -symmetry “friendliness.” The computational basis is well-suited for calculating spectra and correlation functions of local operators for Hamiltonians (like that of the XXZ model) that preserve the total magnetization in z direction.

However, the computational basis appears poorly equipped to describe states with nontrivial topology, such as chiral states, current-carrying states, or states with windings. One prominent example is the spin-helix state in a one-dimensional spin chain,

$$|\Psi(\alpha_0, \eta)\rangle = \bigotimes_n |\phi(\alpha_0 + n\eta)\rangle, \quad (1)$$

where $|\phi(\alpha)\rangle$ describes the state of a qubit, while $+n\eta$ represents the linear increase of the qubit phase along the chain, parametrized in a proper model-dependent way. Thanks to their factorizability, spin helices (1) are straightforward to prepare in experimental setups that allow for an adjustable spin exchange, such as those involving cold atoms [2–4]. These helices possess interesting properties as evidenced by both experimental [2–4] and theoretical [5–8] studies. It was suggested that quantum states with helicity

are even better protected from noise than the ground state, and that the helical protection extends over intermediate timescales [9].

Since the spin-helix state (1) is not an eigenstate of the operator of the total magnetization, it is not confined to a single $U(1)$ block, but is given by a sum over all the blocks, with fine-tuned coefficients, as shown in (9) and (10), even for spatially homogeneous spin helices [$\eta = 0$ in (1)]. A simple shift of the helix phase, $\alpha_0 \rightarrow \alpha_0 + \text{const}$ in (1), gives a linearly independent state with the same qualitative properties (winding, current, etc.). However, to represent such a shift in the standard computational basis, all the fine-tuned expansion coefficients must be changed in a different manner.

We shall introduce an alternative basis, all components of which are chiral themselves and thus ideally tailored for the description of chiral states. This chiral basis consists of helices and helices with kinks (phase dislocations). It provides a block hierarchy based on the number of kinks (rather than on the number of down spins as in case of the computational basis). Unlike the computational basis, the chiral basis is intrinsically topological.

We diagonalize the XX Hamiltonian in the chiral basis and apply the chiral eigenbasis to the problem of spin-helix decay under XX dynamics. This is a problem of its own relevance for experiment [2,4] and theory. Except for some quench problems, only very few explicit examples [10–12] of exact nonequilibrium dynamics of many-body quantum systems are known. Those examples rely on the summation of series of matrix elements and overlaps of initial states with Bethe eigenstates. Although the latter are known in our spin-helix case [13], their summation has remained a problem. The chiral basis helps to circumvent this problem, as we have other selection rules for the matrix elements and obtain particularly convenient forms of the overlaps. Unlike

previous works [8,14] that dealt with the simpler case of spin helices modulated in the XZ plane, we deal with transverse spin helices modulated in the XY plane. Longitudinal and transverse spin helices behave rather differently. In particular, transverse helices can exhibit quantum scars [15] under XXZ dynamics.

Chiral multiqubit basis.—Our starting point is the “winding number operator”

$$V = \frac{1}{4} \sum_{k=1}^{N/2} (\sigma_{2k-1}^x \sigma_{2k}^y - \sigma_{2k}^y \sigma_{2k+1}^x), \quad (2)$$

defined for an even number of qubits N . It has remarkably simple factorized eigenstates. A state

$$\Psi = \varphi_1 \otimes \zeta_1 \otimes \varphi_2 \otimes \zeta_2 \otimes \dots \otimes \varphi_{N/2} \otimes \zeta_{N/2} \quad (3)$$

is an eigenstate of V , if all odd (even) qubits are polarized in positive or negative x (y) direction,

$$\langle \varphi_j | = \frac{1}{\sqrt{2}} (1, \pm 1), \quad \langle \zeta_j | = \frac{1}{\sqrt{2}} (1, \mp i). \quad (4)$$

In such states the qubit polarization at each link between n , $n+1$ changes by an angle of $+\pi/2$ or $-\pi/2$ in the XY plane. Each anticlockwise or clockwise rotation by $\pi/2$ adds $+1$ or -1 to the eigenvalue of $4V$ so that

$$V\Psi = \frac{1}{4} (N - 2M)\Psi, \quad (5)$$

where M is the number of clockwise rotations, further referred to as “kinks.” Clearly, every state Ψ in (3) is uniquely characterized by the kink positions $1 \leq n_1 < \dots < n_M \leq N$ (between qubits n_k , $n_k + 1$), and the polarization $\kappa = \pm$ of the first qubit φ_1 . We denote this state by $i \sum_{\kappa} | \kappa; \mathbf{n} \rangle$, where $\mathbf{n} = (n_1, \dots, n_M)$. Then, by construction, the set of V eigenstates

$$\{ | \kappa; \mathbf{n} \rangle | \kappa = \pm, 1 \leq n_1 < \dots < n_M \leq N \} \quad (6)$$

is an orthonormal basis of N qubits that we call the chiral basis. For compatibility with periodic boundary conditions the winding number $(N - 2M)/4$ must be an integer, implying that M must be even (odd) if $N/2$ is even (odd). We shall call such values of M admissible.

Remark 1.—The chiral basis vectors have a topological nature; a single kink cannot be added to (removed from) a periodic chain by the action of a local operator. In an open chain this is only possible at the boundary.

Remark 2.—Applying σ_n^z in a kink-free zone creates a kink pair at the neighboring positions $n-1$ and n . Applying a string of operators $\sigma_n^z \sigma_{n+1}^z \dots \sigma_{n+k}^z$ in a kink-free zone creates two kinks at a distance of $k+1$, e.g.,

$$| +; 1, k+2 \rangle = \sigma_2^z \sigma_3^z \dots \sigma_{k+2}^z | + \rangle, \quad (7)$$

where $| + \rangle$ is a perfect spin helix of type (1),

$$| + \rangle = | \rightarrow \uparrow \leftarrow \downarrow \rightarrow \uparrow \leftarrow \downarrow \dots \rangle, \quad (8)$$

i.e., a spin helix with maximal winding number $N/4$. Here, the arrows depict the polarization of the qubits in the XY plane, e.g., \uparrow, \downarrow depict a qubit ζ_j (4) with polarization along the y axis.

Remark 3.—The connection between the chiral basis and the standard computational basis is nontrivial. For example, the chiral vacuum state (8) is expanded in terms of the computational basis as

$$| + \rangle = 2^{-\frac{N}{2}} \sum_{n=0}^N (-i)^n \xi_n, \quad (9)$$

$$\xi_n = \frac{1}{n!} \sum_{l_1, \dots, l_n=1}^N i^{l_1 + \dots + l_n} \sigma_{l_1}^- \dots \sigma_{l_n}^- \begin{pmatrix} 1 \\ 0 \end{pmatrix}^{\otimes N}; \quad (10)$$

see [5] for a proof.

In the following we will explore two applications of the chiral basis that are related. First, we will use it to classify the eigenstates of the XX model according to the number of kinks.

Eigenstates of the XX model within the chiral sectors.—The crucial observation is that V commutes with the Hamiltonian of the XX model,

$$H = \sum_{n=1}^N \sigma_n^x \sigma_{n+1}^x + \sigma_n^y \sigma_{n+1}^y, \quad \vec{\sigma}_{N+1} \equiv \vec{\sigma}_1. \quad (11)$$

Consequently, H is block diagonal in the chiral basis with each block corresponding to a fixed number of kinks M . For one-kink states $M=1$ we obtain

$$H | \kappa; n \rangle = 2 | \kappa; n-1 \rangle + 2 | \kappa; n+1 \rangle, \quad n \neq 1, N,$$

$$H | \kappa; 1 \rangle = -2 | -\kappa; N \rangle + 2 | \kappa; 2 \rangle,$$

$$H | \kappa; N \rangle = -2 | -\kappa; 1 \rangle + 2 | \kappa; N-1 \rangle.$$

The $2N$ eigenstates of H belonging to the one-kink subspace are given by the ansatz

$$| \mu_1(p) \rangle = \frac{1}{\sqrt{2N}} \sum_{n=1}^N e^{ipn} (| +; n \rangle - e^{ipN} | -; n \rangle), \quad (12)$$

$$e^{ipN} = \pm 1, \quad (13)$$

where p is a chiral analog of the quasimomentum. The diagonalization of H within a subspace with an arbitrary number of kinks can be performed by the coordinate Bethe

ansatz (see [16]), which gives a complete set of eigenvectors in the chiral basis.

Theorem.—The states

$$\begin{aligned}
 |\mu_M(\mathbf{p})\rangle &= \sum_{1 \leq n_1 < \dots < n_M \leq N} \chi_{\mathbf{n}}(\mathbf{p}) \{|1; \mathbf{n}\rangle - e^{ip_1 N} | -1; \mathbf{n}\rangle\}, \\
 \chi_{\mathbf{n}}(\mathbf{p}) &= \frac{1}{\sqrt{2N^M}} \det_{j,k=1,\dots,M} \{e^{ip_j n_k}\}, \\
 |u; \mathbf{n}\rangle &= (-i)^{\sum_{j=1}^M n_j} \bigotimes_{k=1}^{n_1} \psi_k(u) \bigotimes_{k=n_1+1}^{n_2} \psi_k(u+2) \\
 &\quad \dots \bigotimes_{k=n_M+1}^N \psi_k(u+2M), \\
 \psi_k(u) &= \frac{1}{\sqrt{2}} \begin{pmatrix} 1 \\ e^{i\frac{\pi}{2}(k-u)} \end{pmatrix}, \quad (14)
 \end{aligned}$$

where M is admissible and where the chiral quasimomenta $\mathbf{p} = (p_1, p_2, \dots, p_M)$ satisfy either $e^{ip_j N} = 1$ or $e^{ip_j N} = -1$ for all p_j , form an orthonormal basis of eigenstates of Hamiltonian (11), $\langle \mu_M(\mathbf{p}) | \mu_{M'}(\mathbf{p}') \rangle = \delta_{\mathbf{p}, \mathbf{p}'} \delta_{M, M'}$. The corresponding energy eigenvalues are $E_{\mathbf{p}} = \sum_{j=1}^M \varepsilon_{p_j}$, $\varepsilon_p = 4\cos(p)$.

Some clarifications might be appropriate here. First, the states (14) are a generalization of those in (6) by an additional rotation of all qubits by the same angle $\pi(1-u)/2$ in the XY plane. Setting $u = 1$ yields (6). The extra degree of freedom originates from the $U(1)$ symmetry of the XX model.

Second, the XX eigenstates in the chiral basis formally resemble those in the usual computational basis [18], where the number of spins up plays the role of the number of kinks. In particular, the wave functions $\chi_{\mathbf{n}}(\mathbf{p})$ have the familiar form of Slater determinants.

Spin-helix decay in the XX model.—Next, we apply our chiral basis to study the time evolution of a transverse spin-helix magnetization profile, measured in [2]. We are able to obtain an exact and explicit answer, when the time evolution of the local spin $\vec{\sigma}_n(t) = e^{iHt} \vec{\sigma}_n e^{-iHt}$ is driven by the XX Hamiltonian (11). The initial spin helix in the XY plane is described by the state

$$|\Psi_Q\rangle = \frac{1}{\sqrt{2^N}} \bigotimes_{n=1}^N \begin{pmatrix} e^{-i\frac{Qn}{2}} \\ e^{i\frac{Qn}{2}} \end{pmatrix}, \quad (15)$$

where the wave vector Q satisfies the commensurability condition $QN = 0 \pmod{2\pi}$. Setting $\Phi = \sum_{n=1}^N Qn\sigma_n^z$ and $|\Omega\rangle = |\Psi_0\rangle$ we see that $|\Psi_Q\rangle = e^{-(i\Phi/2)} |\Omega\rangle$. The operator $e^{-(i\Phi/2)}$ induces a rotation of qubits at site n about the z axis by an angle Qn . Thus,

$$\langle \Psi_Q | \vec{\sigma}_n | \Psi_Q \rangle = \langle \Omega | e^{i\frac{Qn}{2}} \vec{\sigma}_n e^{-i\frac{Qn}{2}} | \Omega \rangle = \begin{pmatrix} \cos(Qn) \\ \sin(Qn) \\ 0 \end{pmatrix}, \quad (16)$$

which is precisely a spin helix in the XY plane. In order to obtain its time evolution we have to replace $\vec{\sigma}_n$ by $\vec{\sigma}_n(t)$ in (16) and commute $e^{(i\Phi/2)}$ through H . The details of this calculation can be found in [16,19]. We finally obtain a remarkably simple structure:

$$\langle \Psi_Q | \vec{\sigma}_n(t) | \Psi_Q \rangle = S_N(\cos(Q)t) \begin{pmatrix} \cos(Qn) \\ \sin(Qn) \\ 0 \end{pmatrix}, \quad (17)$$

$$S_N(t) = \langle \Omega | \sigma_1^x(t) | \Omega \rangle. \quad (18)$$

The shape of the magnetization profile is not changing with time. The profile fades away with an amplitude

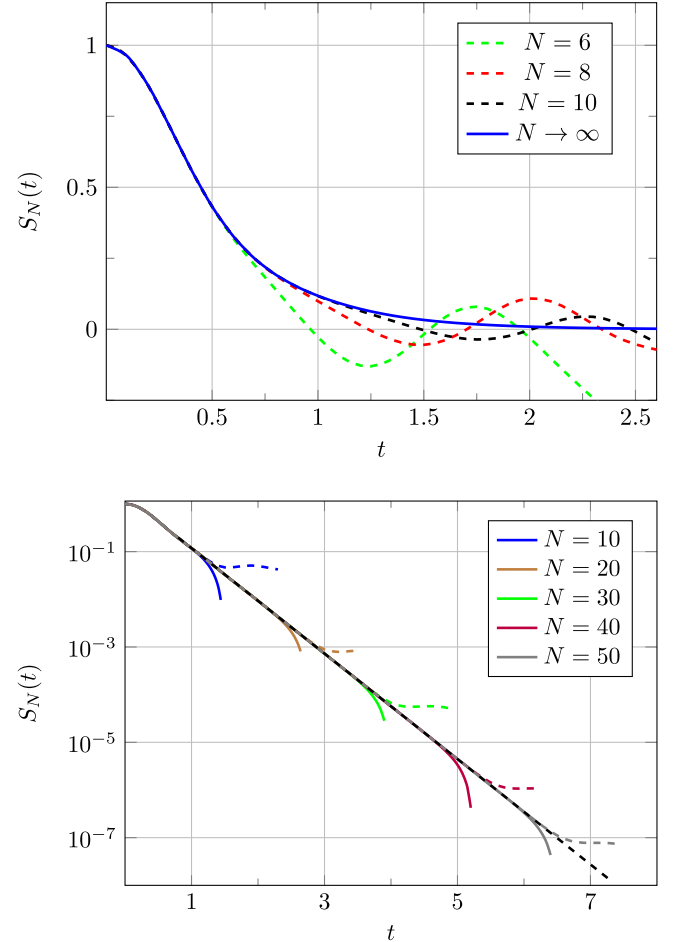


FIG. 1. Universal relaxation function of the spin-helix amplitude (18) for different system sizes, in usual scale (top panel) and in logarithmic scale (bottom panel). Top panel: green, red, and black dots correspond to $S_6(t)$, $S_8(t)$, $S_{10}(t)$, respectively, while the continuous curve shows $S(t)$ (24). The blue line is to be compared with Fig. 2(a) in [2]. Bottom panel: $S_N(t)$ for $N = 10, 20, \dots, 50$, from (23), shows the exponential decay for large times, given by the black dashed line, (33). Colored dashed curves show $S(r, t)$ with $r = [N/4]$ from (29). Curves with the same color code correspond to the same N . Deviations from the straight line at large t are due to finite size effects.

$S_N(\cos(Q)t)$, which depends on the wave vector Q in a self-similar way.

The remaining universal function $S_N(t)$ is still a non-equilibrium one-point function and therefore hard to calculate. Free fermion techniques involving a Jordan-Wigner transformation do not seem to sufficiently simplify the problem because the density matrix associated with $|\Omega\rangle$ is not an exponential of bilinear expressions in Fermi operators c_j, c_j^\dagger ; see [20]. As previously seen in other examples [18,21] an appropriately adapted Bethe ansatz technique, in the present case based on the chiral basis, turns out to be more efficient.

A key simplification in calculating $S_N(t)$ by means of the chiral basis consists in the fact that, with $u = 1$ in (14), the operator σ_1^x becomes diagonal in the chiral basis

$$\sigma_1^x |\pm; \mathbf{n}\rangle = \pm |\pm; \mathbf{n}\rangle \quad (19)$$

for all admissible M , leading to

$$\langle \mu_{M'}(\mathbf{q}) | \sigma_1^x | \mu_M(\mathbf{p}) \rangle = 0, \quad \text{if } M \neq M'. \quad (20)$$

Inserting $I = \sum_{\mathbf{p}, M} |\mu_M(\mathbf{p})\rangle \langle \mu_M(\mathbf{p})|$ in (18) and using (20) we obtain

$$S_N(t) = \sum_{\mathbf{p}, \mathbf{q}, M} e^{i(E_{\mathbf{p}} - E_{\mathbf{q}})t} \times \langle \Omega | \mu_M(\mathbf{p}) \rangle \langle \mu_M(\mathbf{p}) | \sigma_1^x | \mu_M(\mathbf{q}) \rangle \langle \mu_M(\mathbf{q}) | \Omega \rangle. \quad (21)$$

We also find that $\langle \Omega | \mu_M(\mathbf{p}) \rangle = 0$ unless $M = N/2$. After an explicit evaluation of the matrix elements and the overlaps and after performing the necessary summations (see [16]) we eventually obtain

$$S_N(t) = \text{Re} \left\{ \det_{m,n=1,\dots,N/2} \phi_{m,n}^{(N)}(t) \right\}, \quad (22)$$

$$K_{m,n}(t) = \frac{t}{m-n} (J_{2m}(4t)J_{2n-1}(4t) - J_{2n}(4t)J_{2m-1}(4t)) + \frac{t}{m-n} (J_{2m-1}(4t)J_{2n-2}(4t) - J_{2n-1}(4t)J_{2m-2}(4t)) \\ + \frac{it}{m-n-1/2} (J_{2m-2}(4t)J_{2n}(4t) - J_{2n-1}(4t)J_{2m-1}(4t)) - \frac{it}{m-n+1/2} (J_{2m-1}(4t)J_{2n-1}(4t) - J_{2n-2}(4t)J_{2m}(4t)), \\ K_{n,n}(t) = -(J_0(4t))^2 + (J_{2n-1}(4t))^2 + 2 \sum_{j=0}^{2n-2} (J_j(4t))^2, \quad (27)$$

where the $J_k(x)$ are Bessel functions. After further manipulations (see [16]) and taking into account the symmetries of $K_{n,m}$ we finally obtain

$$S(t) = \lim_{r \rightarrow \infty} S(r, t), \quad (28)$$

$$S(r, t) = \left| \det_{m,n=1,\dots,r} A_{m,n}(t) \right|^2, \quad (29)$$

$$\phi_{m,n}^{(N)}(t) = \sum_{\substack{p \in B_+ \\ q \in B_-}} \frac{(1 + e^{-ip})(1 + e^{iq})e^{i[2(m-p-nq)+t(\varepsilon_p - \varepsilon_q)]}}{N^2(e^{i(p-q)} - 1)}, \quad (23)$$

where B_{\pm} are the sets of $p \in [-\pi, \pi)$ satisfying $e^{ipN} = \pm 1$. Equation (22) describes the relaxation of the helix amplitude for finite periodic systems. Explicit expressions for $S_N(t)$ for $N = 4, 6$ are given in [16].

Analyzing the Taylor expansion of $S_N(t) = \sum_n C_n^{(N)} t^n$ at $t = 0$ we observe that the Taylor coefficients $C_n^{(N)}$ stabilize for fixed n and large N . More precisely, $C_n^{(N+2)} = C_n^{(N)}$ for $n = 0, 1, \dots, 2N - 4$. Consequently, the stable pattern gives the exact Taylor expansion about $t = 0$ of the decay of the spin-helix amplitude in the thermodynamic limit

$$S(t) = \lim_{N \rightarrow \infty} S_N(t), \quad (24)$$

$$S(t) = 1 - 4t^2 + \frac{2^5}{3}t^4 - \frac{2^6}{3}t^6 + \frac{2^9}{15}t^8 - \frac{2^{11}}{45}t^{10} \\ + \frac{2^{12} \times 179}{14\,175}t^{12} - \frac{2^{16} \times 11}{14\,175}t^{14} + \frac{2^{16} \times 2987}{4\,465\,125}t^{16} \\ - \frac{2^{20} \times 143}{4\,465\,125}t^{18} + \dots, \quad (25)$$

obtainable also by direct operatorial methods.

Reduction to Bessel functions.—For large N the sums in (23) can be replaced by integrals. Then, after some algebra, we find (see [16]) that the matrix entries $\phi_{m,n}^{(N)}(t)$ converge to

$$(-1)^{m-n} \phi_{m,n}(t) = \delta_{m,n} + K_{m,n}(t), \quad (26)$$

$$A_{m,n}(t) = \delta_{m,n} + K_{m,n}(t) + K_{m,1-n}(t). \quad (30)$$

These formulas represent $S(t)$ as a product of two infinite determinants. Infinite determinants [22] may define functions in very much the same way as series or integrals. As in the present case, they may be extremely efficient in computations [23]. With a few lines of *Mathematica* code

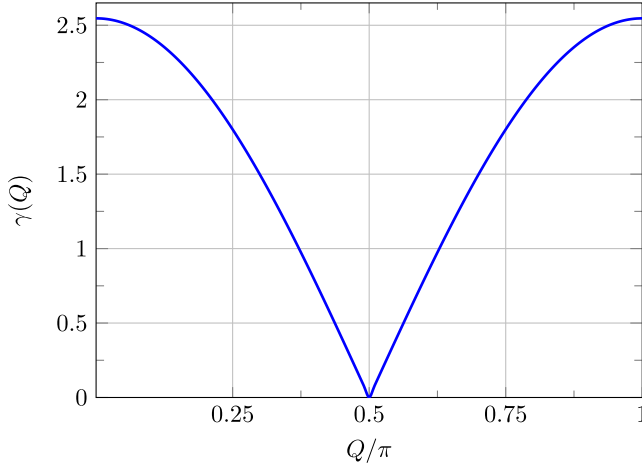


FIG. 2. Asymptotic decay rate γ of the spin-helix state versus rescaled wave vector $k = Q/\pi$, given by $(8/\pi)|\cos(\pi k)|$. This figure is to be compared with the experimental data shown in Fig. 3(c) of [2].

we obtain, e.g., $S(t = 50) = 7.64483 \times 10^{-56}$ within a few seconds on a laptop computer. Unlike the Taylor series (25), the determinant representation determines $S(t)$ for *all* times. The function $S(t)$ shown in Fig. 1 is directly comparable with the experimental data, Fig. 2(a) in [2].

Even though the true thermodynamic limit is given by $r \rightarrow \infty$ in (28), already for $r = 1$, when the matrix A is a scalar, the function

$$S(1, t) = g_0^2 + 4t^2 \left(g_0 + \frac{g_1}{3} \right)^2, \quad g_n = J_n^2(4t) + J_{n+1}^2(4t) \quad (31)$$

approximates $S(t)$ for $0 \leq t \leq 0.5$ (data not shown), and also reproduces the asymptotic Taylor expansion (25) up to the order t^7 .

Choosing $r = 4$ in (29) reproduces $S(t)$ with accuracy $|S(4, t) - S(t)| < 10^{-5}$, for $t < 2$, which is enough for any practical purpose. Indeed at $t = t_{\max} = 2$, the amplitude $S(t)$ drops by 2 orders of magnitude with respect to the initial value, $S(t_{\max}) \approx 0.0093 < S(0)/100$. For larger t , $S(t)$ is well-approximated by the asymptotics (33).

In addition, our numerics suggests a simple asymptotics for $\det A(t)$, namely

$$\det A(t) \rightarrow a_0 e^{2it} e^{-\frac{4}{\pi}t}, \quad t \gg 1, \quad a_0 = 1.2295 \pm 2 \times 10^{-5}. \quad (32)$$

The data were obtained by analyzing $\det A(t)$ for $r \leq 170$, and for times $t < t_m(r) = r/2.2 - 0.19$, data shown in [16]. Equation (32) corresponds to the $S(t)$ asymptotics

$$\lim_{t \rightarrow \infty} S(t) \approx 1.5117 e^{-\frac{8}{\pi}t}. \quad (33)$$

Using that $S(t)$ is even [19] we readily get the spin-helix state decay rate from the asymptotics (33) and the self-similarity (17)

$$\gamma(Q) = -\lim_{t \rightarrow \infty} (t^{-1} \log \langle \sigma_n^x(t) \rangle_Q) = \frac{8}{\pi} |\cos(Q)| \quad (34)$$

shown in Fig. 2 and directly comparable with the experimental result, Fig. 3(c) of [2].

Conclusions.—In this Letter we propose a chiral qubit basis that possesses topological properties while retaining a simple factorized structure and orthonormality. The chiral basis at every site is represented by a pair of mutually orthogonal qubit states and can be implemented with usual binary code registers. We demonstrate the effectiveness of the chiral basis by applying it to an experimentally relevant physical problem. Our results in Figs. 1 and 2 are comparable to the experimental data.

We discovered a universal function $S(t)$ that governs the relaxation of transversal spin helices with arbitrary wavelengths in an infinite system under XX dynamics. We obtained the explicit determinantal form (28) of $S(t)$ and calculated its Taylor expansion (25) and its large- t asymptotics (33). The possibility to express correlation functions in determinantal form is typical of integrable systems; see, e.g., [18,21,24–27]. We also obtained explicit expressions for the spin-helix state relaxation of finite systems of qubits (22) that may be useful to interpret future experiments with ring-shaped atom arrays [28], where periodic boundary conditions can be realized.

The chiral basis can be used to diagonalize any other Hamiltonian that commutes with the winding number operator V , Eq. (2). An important example is the anisotropic XY Hamiltonian for which we expect to be able to obtain efficient formulas for the overlaps and, most likely, also for the relaxation of spin helices. As for the construction of the chiral basis, a generalization to the XYZ case has been put forward in parallel to this work by three of the authors and was recently published in [29].

Financial support from Deutsche Forschungsgemeinschaft through DFG Project No. KL 645/20-2 is gratefully acknowledged. V.P. acknowledges support by the European Research Council (ERC) through the advanced Grant No. 694544—OMNES. X.Z. acknowledges financial support from the National Natural Science Foundation of China (No. 12204519).

- [1] S. Mallat, *A Wavelet Tour of Signal Processing: The Sparse Way*, 3rd Revised edition (Academic Press, London, 2009), <https://dl.icdst.org/pdfs/files/3/64cb10c8a275e5aad045094c29c036e2.pdf>.
 [2] P.N. Jepsen, Y.K. Lee, H. Lin, I. Dimitrova, Y. Margalit, W.W. Ho, and W. Ketterle, *Nat. Phys.* **18**, 899 (2022).

- [3] P.N. Jepsen, J. Amato-Grill, I. Dimitrova, W.W. Ho, E. Demler, and W. Ketterle, *Nature (London)* **588**, 403 (2020).
- [4] P.N. Jepsen, W.W. Ho, J. Amato-Grill, I. Dimitrova, E. Demler, and W. Ketterle, *Phys. Rev. X* **11**, 041054 (2021).
- [5] V. Popkov, X. Zhang, and A. Klümper, *Phys. Rev. B* **104**, L081410 (2021).
- [6] X. Zhang, A. Klümper, and V. Popkov, *Phys. Rev. B* **103**, 115435 (2021).
- [7] X. Zhang, A. Klümper, and V. Popkov, *Phys. Rev. B* **104**, 195409 (2021).
- [8] G. Cecile, S. Gopalakrishnan, R. Vasseur, and J. De Nardis, *Phys. Rev. B* **108**, 075135 (2023).
- [9] S. Kühn, F. Gerken, L. Funcke, T. Hartung, P. Stornati, K. Jansen, and T. Posske, *Phys. Rev. B* **107**, 214422 (2023).
- [10] E. Barouch, B. M. McCoy, and M. Dresden, *Phys. Rev. A* **2**, 1075 (1970).
- [11] H. Moriya, R. Nagao, and T. Sasamoto, *J. Stat. Mech.* (2019) 063105.
- [12] E. Granet, H. Dreyer, and F. H. L. Essler, *SciPost Phys.* **12**, 019 (2022).
- [13] Y. Jiang and B. Pozsgay, *J. High Energy Phys.* 06 (2020) 022.
- [14] D. Pereira and E. J. Mueller, *Phys. Rev. A* **106**, 043306 (2022).
- [15] S. Moudgalya, B. A. Bernevig, and N. Regnault, *Rep. Prog. Phys.* **85**, 086501 (2022).
- [16] See Supplemental Material at <http://link.aps.org/supplemental/10.1103/PhysRevLett.132.220404> for technical details, which includes Ref. [17].
- [17] A. Borodin, A. Okounkov, and G. Olshanski, *J. Am. Math. Soc.* **13**, 481 (2000).
- [18] F. Colomo, A. G. Izergin, V. E. Korepin, and V. Tognetti, *Theor. Math. Phys.* **94**, 11 (1993).
- [19] V. Popkov, M. Žnidarič, and X. Zhang, *Phys. Rev. B* **107**, 235408 (2023).
- [20] F. Ares, S. Murciano, and P. Calabrese, *Nat. Commun.* **14**, 2036 (2023).
- [21] F. Göhmann, K. K. Kozłowski, and J. Suzuki, *J. Math. Phys. (N.Y.)* **61**, 013301 (2020).
- [22] B. Simon, *Adv. Math.* **24**, 244 (1977).
- [23] F. Bornemann, *Math. Comput.* **79**, 871 (2010).
- [24] A. Lenard, *J. Math. Phys. (N.Y.)* **5**, 930 (1964).
- [25] V. E. Korepin and N. A. Slavnov, *Commun. Math. Phys.* **129**, 103 (1990).
- [26] F. Göhmann, R. Kleinemühl, and A. Weiße, *J. Phys. A* **54**, 414001 (2021).
- [27] C. Babenko, F. Göhmann, K. K. Kozłowski, J. Sirker, and J. Suzuki, *Phys. Rev. Lett.* **126**, 210602 (2021).
- [28] P. Scholl, H. J. Williams, G. Bornet, F. Wallner, D. Barredo, L. Henriot, A. Signoles, C. Hainaut, T. Franz, S. Geier *et al.*, *PRX Quantum* **3**, 020303 (2022).
- [29] X. Zhang, A. Klümper, and V. Popkov, *Phys. Rev. B* **109**, 115411 (2024).